Available online at www.sciencedirect.com
SCIENCE DIRECT
Journal of Catalysis 239 (2006) 137–144
JOURNAL OF CATALYSIS
www.elsevier.com/locate/jcat

Quenching of potassium loss from styrene catalyst: Effect of Cr doping on stabilization of the $K_2Fe_{22}O_{34}$ active phase

Irmina Serafin [a], Andrzej Kotarba [a,*], Maciej Grzywa [a], Zbigniew Sojka [a,b], Halina Bińczycka [c], Piotr Kuśtrowski [a]

[a] *Faculty of Chemistry, Jagiellonian University, Ingardena 3, 30-060 Cracow, Poland*
[b] *Regional Laboratory of Physicochemical Analyses and Structural Research, Ingardena 3, 30-060 Cracow, Poland*
[c] *Faculty of Physics, Astronomy and Applied Computer Science, Jagiellonian University, Reymonta 4, 30-059 Cracow, Poland*

Received 29 November 2005; revised 17 January 2006; accepted 20 January 2006

Available online 17 February 2006

Abstract

The stabilization of potassium in β-ferrite, the active phase of styrene catalyst by chromium additive (0.25–5 wt%), was investigated by means of a species-resolved (K and K^+) thermal alkali desorption technique, corroborated by XRD, Mössbauer, XPS, SEM characterization, and reactivity studies. The Mössbauer spectra revealed that a major part of Cr^{3+} substitutes the Fe^{3+} ions in the octahedral (12 k) positions. Introduction of chromium causes an increase in desorption energy by 1.1 eV for potassium ions and by 1.4 eV for potassium atoms. The stabilizing effect of chromium has been explained in terms of the extra-pillars potassium-blocking model, which involves the displacement of Fe^{3+} ions into 4f tetrahedral positions, leading to the formation of additional iron oxide pillars between the spinel blocks of the β-ferrite. The appearance of topological constrains prevents potassium diffusion in the [001] conduction plane to an external surface. As a result, at the process temperature (600–650 °C), the volatilization of potassium from β-ferrite is significantly quenched, while the activity in ethylbenzene dehydrogenation is simultaneously enhanced.

Keywords: Styrene catalyst; Potassium ferrites; Potassium loss; Chromium; Diffusion

1. Introduction

Catalytic dehydrogenation of ethylbenzene (EBDH) to produce styrene accounts for >90% of the worldwide capacity, with 25 million tons of monomer produced annually [1]. The industrial process is performed at temperatures as high as 823–973 K in excess steam over potassium-promoted iron oxide catalysts [2]. Promotion with potassium increases the activity of the catalyst by an order of magnitude. Although the commercial catalysts are very active and selective, the severe process conditions give rise to steady deterioration and the need for catalyst replacement in the installation every 1–2 years. Consequently, great emphasis has been placed on developing chemically stable and mechanically robust catalysts for this application. The main reasons for the activity decay during the time on stream operation are deposition of excessive carbon and the loss of potassium promoter [3]. To avoid excessive carbon deposition, steam is cofed to the reactant stream for coke removal, whereas to improve potassium stability and prolong the lifetime of the catalyst, solid-state doping with alien metal ions is used in industrial practice.

It is well known that adding Cr_2O_3 to the iron oxide catalysts enhances their activity and discourages sintering [4–7]. The traditional catalyst precursors that have dominated the market for many years are composed of $Fe_2O_3/Cr_2O_3/K_2CO_3$ [8]. Common structural additives to industrial catalysts include Ce [9,10], Mo [10], and Al [11]. Recently, promising results were reported on a Mn additive, which not only increases the number of EBDH active sites [12], but also stabilizes $K_2Fe_{22}O_{34}$ ferrite, one of the active phases of the catalyst [13].

Extensive research has been dedicated to improving understanding of the active state of the iron oxide catalyst surface

* Corresponding author.
E-mail address: kotarba@chemia.uj.edu.pl (A. Kotarba).

0021-9517/$ – see front matter
doi:10.1016/j.jcat.2006.01.026

as well as of potassium loss, the most serious irreversible deactivating process. Recently, a species-resolved thermal alkali desorption (SR-TAD) method was applied to monitor the loss of K and K^+ from the model phases present in the life cycle of EBDH catalyst. The interaction of potassium with the iron oxide matrix is complex, and the active state of the catalysts has been assigned to the equilibrium between two ferrite phases, $KFeO_2 \leftrightarrows K_2Fe_{22}O_{34}$, as discussed by Muhler and Schlögl [11,14,15]. Among these, β-ferrite ($K_2Fe_{22}O_{34}$) was explicitly identified as being principally responsible for potassium volatilization from the catalyst [16].

The aim of the present study was to explore the effect of chromium as a stabilizer of potassium in β-ferrite, the active phase of styrene catalyst. We synthesized a model β-ferrite phase doped with Cr ions and characterized it by various methods, including X-ray diffraction (XRD), scanning electron microscopy (SEM), X-ray photoelectron spectroscopy (XPS), and Mössbauer spectroscopy, to ascertain the structure and surface composition of the resultant material. Potassium volatility was evaluated in terms of both K and K^+ desorption fluxes and their energetics, and confronted with the effect of chromium on the activity of β-ferrite in the EBDH reaction. A solid-state model of the Cr-doped β-ferrite was developed to account for the observed potassium stabilization effect.

2. Experimental

The samples of undoped $K_2Fe_{22}O_{34}$ ferrite were prepared by solid-state reaction of a stoichiometric mixture of K_2CO_3 with α-Fe_2O_3 at 1470 K as described previously [17]. For 0.25–5 wt% Cr-doped samples, the apposite part of α-Fe_2O_3 was replaced by Cr_2O_3.

The phase composition of the resultant β-ferrite was verified after synthesis by XRD using a Philips X'pert Pro powder diffractometer with Co-K_α radiation in the Bragg–Brentano geometry. The Mössbauer experiments were performed in transmission geometry at room temperature using a constant acceleration drive. A source of ^{57}Co in Rh with activity of 10 mCi was used. The velocity scale of the Mössbauer spectra and all isomer shifts (ISs) were calibrated with respect to the reference spectrum of metallic iron.

The surface morphology was examined by SEM using a Philips XL 30 scanning electron microscope at 10,000× magnification. The surface composition was studied by XPS using a Vacuum Systems Workshop instrument equipped with a concentric hemispherical 150-mm electron analyzer and a two-plate 18-channel detector (Galileo). The electron analyzer was operated in fixed-analysis transmission (FAT) with a constant pass energy of 22.5 eV. An Al anode with K_α (1486.6 eV) radiation of 200 W served as the X-ray source. The background pressure during the experiments was $>5 \times 10^{-8}$ mbar. Calibration of the binding energy scale was done with the position of the C 1s line for C–C and C–H bonding at 284.6 eV.

The catalytic tests for ethylbenzene dehydrogenation were carried out in a fix-bed plug-flow microreactor (4.5 mm i.d., 240 mm long) using a 60 mg sample of catalyst with a fraction of particle size 0.2–0.3 mm placed at the central position of the reactor onto a quartz wool plug. The catalyst bed was heated to 550–650 °C by an electrical oven controlled by a temperature controller (Digi-Sense; Cole-Parmer) equipped with a K-type thermocouple placed inside the catalyst bed and protected by a quartz capillary. The carrier He flow rate of 50 ml/min was controlled by a mass flow controller (Brooks 5850^E). Ethylbenzene (100 µl/h) and water (200 µl/h) were fed to the reaction system with syringe pumps (Cole-Parmer). The reaction products and unreacted ethylbenzene were analyzed by gas chromatography (GC) using a Varian CP-3800 gas chromatograph equipped with a capillary column Poraplot Q (Chrompack) and a thermal conductivity detector. Reactant samples were collected directly from the reactor outlet using a six-port valve (Valco).

Before activity testing, the catalyst was kept at 550 °C in a flow of pure helium (50 ml/min) for 30 min and then in He saturated with steam (200 µL water/h) for the next 30 min. Dosing of ethylbenzene began just after the pretreatment, and after 15 min first GC analysis was performed. The temperature of the catalyst bed was ramped up in 50 °C increments, with three analyses of products (at 35-min intervals) done at each step.

The surface stability of potassium was investigated by a SR-TAD method, and the effect of chromium additives was evaluated analogously, as described elsewhere in more detail [16]. The experiments were carried out in a vacuum apparatus with a background pressure of 10^{-7} mbar. The samples, in the form of 10-mm-diameter, 100-mg wafers, were heated from room temperature to 700 °C in a stepwise mode at a rate of 5 °C/min. Previous desorption studies of potassium from styrene catalysts [18–20] and related ferrite phases [16,21] revealed that the K loss occurs in the form of atoms (in the ground and excited states) as well as ions. Therefore, to obtain an integral picture of the promoter stability, we followed both K and K^+ desorption fluxes. The desorption flux of potassium atoms was determined by means of a surface ionization detector [22]; the flux of K^+ ions, simply by using an ion collector. Because ferrites are efficient electron emitters, the samples were biased, with a positive potential (+10 V for K and +60 V for K^+) to quench the thermal emission of electrons and, in the case of K^+, also to accelerate them toward the collector. This approach effectively eliminates the possibility of reneutralization of K^+ ions by thermal electrons outside the surface. In all of the measurements made with a Keithley 6512 digital electrometer, the resultant positive current was averaged over 10 independent data points for each temperature.

3. Results and discussion

3.1. Catalyst characterization

The diffraction patterns of all the undoped and Cr-doped ferrites reveal that the synthesized samples were practically monophasic, composed of $K_2Fe_{22}O_{34}$ (Joint Committee on Powder Diffraction Standards International Centre for Diffraction Data, data card 31-1034). However, in the case of highest Cr-doping (5%), along with the dominant pattern due to $K_2Fe_{22}O_{34}$ (principal lines indexed within the *P63/mmc* space

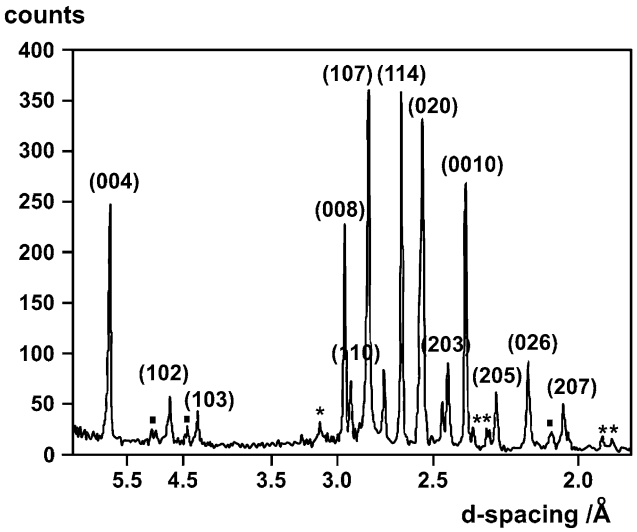

Fig. 1. X-Ray diffraction patterns of 2% Cr-doped $K_2Fe_{22}O_{34}$ ferrite indexed within *P63/mmc* space group. The minor phases of α-Fe_2O_3 and K_2CrO_4 are labelled with (■) and (*), respectively.

group), two sets of weaker lines can be distinguished (Fig. 1), attributed to K_2CrO_4 (*Pnma*) and Fe_2O_3 (R-3C 167) minor phases.

The SEM morphology of the resultant bare and Cr-doped ferrites is shown in Figs. 2a and b. The well-developed plate crystallites of hexagonal shape (0.5–2 μm diameter, ∼0.2 μm thick) resemble those of a single K^+-β-ferrite with stoichiometric composition [17] regardless of chromium content. Because the size of the crystallites assessed from the Debye–Scherrer formula is 0.12 ± 0.03 μm, it can be concluded that the observed particles are composed of about 5–20 soldered crystallites.

Closer inspection of the positions of the 2 and 5% Cr-β-ferrite diffraction peaks reveals that they are slightly shifted in respect to the corresponding undoped sample. This may suggest that chromium has been also incorporated into the lattice of $K_2Fe_{22}O_{34}$. Because the ionic radii of trivalent iron and chromium are similar the XRD are not sufficiently reliable to resolve the problem conclusively, complementary Mössbauer and XPS measurements were performed.

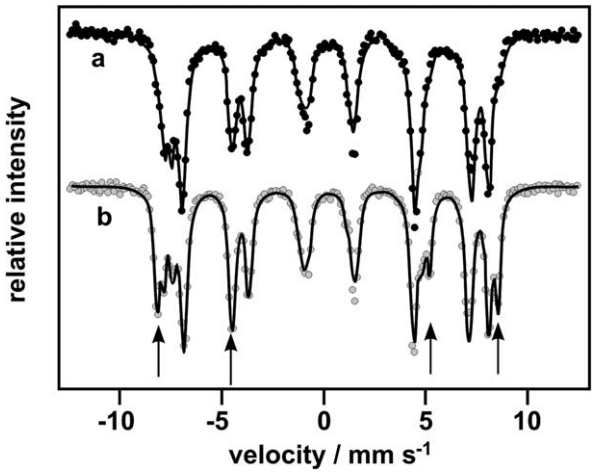

Fig. 3. Mössbauer spectra of (a) undoped and (b) Cr-doped $K_2Fe_{22}O_{34}$.

The Mössbauer spectra for undoped and Cr-doped $K_2Fe_{22}O_{34}$ are presented in Figs. 3a and b and the spectral parameters obtained by computer fitting are collected in Table 1. Potassium ferrite, $K_2Fe_{22}O_{34}$, exhibits a defected spinel structure (Fig. 4a) similar to that of the better-known ionic conductor β-Al_2O_3 [23]. The lattice of the stoichiometric $K_2Fe_{22}O_{34}$ includes four crystallographically distinct Fe sites: two octahedral sites, *Fe1* and *Fe4* (equivalent to *12k* and *2a* in Wyckoff notation), and two tetrahedral sites, *Fe2* and *Fe3* (both equivalent to 4f). Thus the Mössbauer spectrum of this compound should be resolved into four six-line hyperfine patterns assigned to these four sites. The magnetic splitting of 485–491 kOe can be attributed to tetrahedral Fe^{3+} (*Fe2* and *Fe3*), whereas $H = 441$–520 kOe to Fe^{3+} in two octahedral sites (*Fe1* and *Fe4*) (see Fig. 4a and Table 1). The parameters thus obtained are in very good agreement with earlier findings on iron oxide catalysts reported by Muhler et al. [11]. In the case of Cr-doped ferrite, the additional sextet of $H = 515$ kOe characteristic of α-Fe_2O_3 had to be added to fit the experimental spectrum successfully. Such a minute contribution of hematite to β-ferrite has also been observed for another dopants (e.g., magnesium) [24].

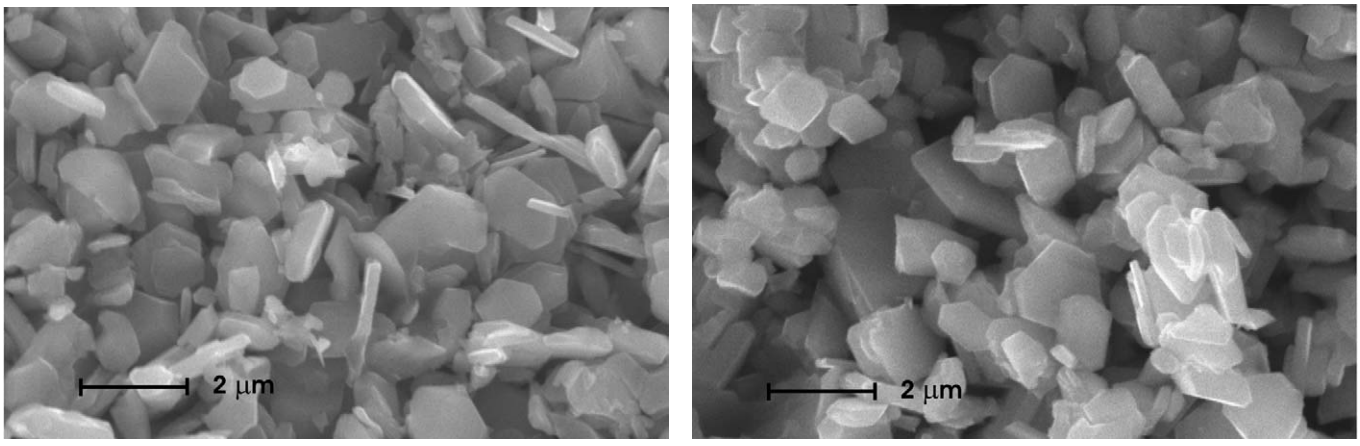

(a) (b)

Fig. 2. SEM (20 kV) images of (a) undoped and (b) 2% Cr-doped $K_2Fe_{22}O_{34}$ ferrite.

Table 1
Mössbauer parameters: isomer shift (IS), quadrupole splitting (QS), magnetic hyperfine field (H), linewidth (Γ), and the ratio of octahedral to tetrahedral sites occupied by Fe^{3+} (o/t) for undoped, 2% and 5% Cr-doped $K_2Fe_{22}O_{34}$

Parameter	Samples													
	$K_2Fe_{22}O_{34}$				2% Cr-$K_2Fe_{22}O_{34}$					5% Cr-$K_2Fe_{22}O_{34}$				
	Fe1	*Fe2*	*Fe3*	*Fe4*	*Fe1*	*Fe2*	*Fe3*	*Fe4*	*Fe5*	*Fe1*	*Fe2*	*Fe3*	*Fe4*	*Fe5*
IS [mm/s]	0.35(1)	0.28	0.21	0.36	0.35	0.26	0.23	0.35	0.37	0.36	0.27	0.23	0.37	0.37
QS [mm/s]	0.11(1)	0.02	−0.15	0.02	0.12	0.05	−0.22	0.07	0.10	0.10	0.07	−0.17	0.09	0.10
H [kOe]	441(1)	496	483	520	435	495	483	524	516	443	496	485	524	516
Γ [mm/s]	0.26(1)	0.17	0.17	0.28	0.22	0.17	0.17	0.13	0.15	0.26	0.19	0.19	0.14	0.13
RA [%]	55(2)	18	17	10	46	16	16	8	14	38	18	15	5	24
o/t	1.86				1.70					1.38				

The surface composition of the bare and Cr-doped β-ferrite was studied by XPS. A typical survey spectrum for Cr-doped $K_2Fe_{22}O_{34}$, together with the narrow scans for Fe 2p and Cr 2p, are shown in Fig. 5, and the corresponding binding energies are collected in Table 2. The survey scan indicates that within the surface layer of investigated samples, with the exception of ubiquitous adventitious carbon, only the constituent elements were found. The observed binding energies for iron, the most diagnostic Fe 2p3/2 region, was dominated by the signal at 710.3, which is characteristic of Fe^{3+} ions in octahedral and tetrahedral positions because these coordinations cannot be distinguished by XPS [25–27]. The wide Fe 2p3/2 line and the presence of a core-level shake-up satellite at 720 eV are consistent with a high spin configuration of iron typical in an O^{2-} environment. The O 1s peak was broad (FWHM = 2.6–1.8 eV), with a shoulder about 1.2 eV above the principal line at 529.6 eV. The same features were previously noted in the oxygen core band and assigned to the presence of hydroxyl groups on iron oxides [19]. The Fe 2p XPS spectrum of $K_2Fe_{22}O_{34}$ was very similar to that observed for the iron oxides, with only the position of the 2p3/2 line shifted slightly to a lower binding energy value. The lack of peak at 709.3 characteristic of Fe^{2+} indicates that, in accordance with the Mössbauer results, the divalent iron is essentially absent in the samples [26]. Unfortunately, because the difference between the Fe^{3+} 2p3/2 in the lattice of ferrite and hematite is too small (∼0.2 eV), these two states of trivalent iron cannot be distinguished. The XPS results for iron were basically in line with findings of previous studies on those systems, although explicit XPS investigations were beyond the scope of this work; a more in-depth analysis of these data has been provided elsewhere [20].

More informative data can be extracted from the chromium narrow scan spectra. The presence of two sets of chromium doublets (2p1/2 and 2p3/2) is consistent with two oxidative states, Cr^{3+} and Cr^{6+}. Whereas the Cr^{6+} is consistent with the presence of potassium-segregated chromate revealed by XRD (Fig. 1), the Cr^{3+} in octahedral coordination in conjunction with the Mössbauer data indicates the substitution of Fe^{3+} for Cr^{3+} in the *Fe1* sites of the β-ferrite phase.

3.2. *Effect of chromium doping on catalytic activity of β-ferrite*

Because chromium is added to the styrene catalyst as a stabilizer and also as an activity enhancer, these two function must be verified in the particular case of the β-ferrite active phase. Both the bare and 2% Cr-doped $K_2Fe_{22}O_{34}$ ferrites proved their activity in ethylbenzene dehydrogenation (Fig. 6). At all

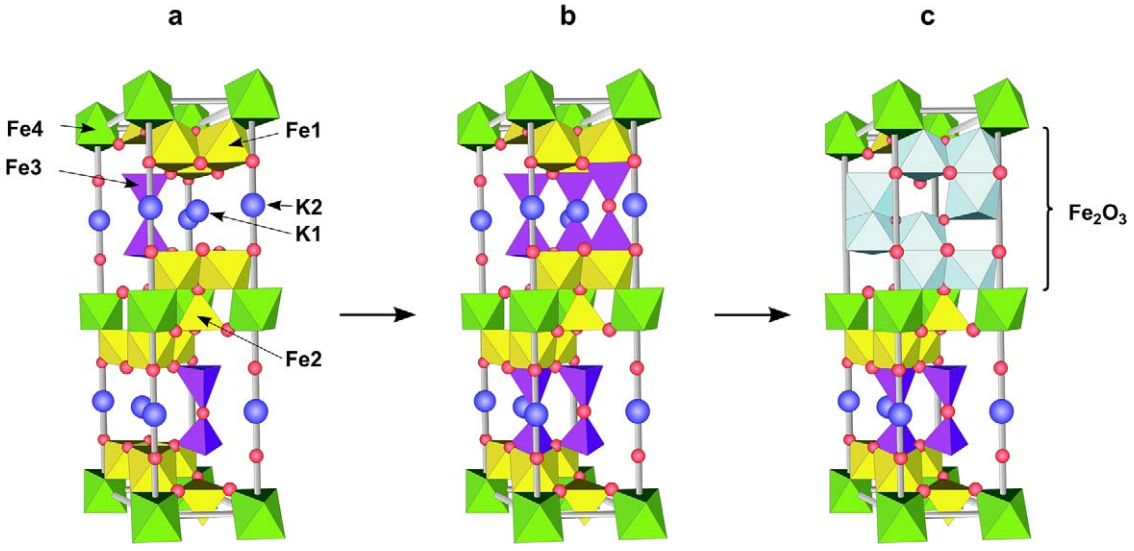

Fig. 4. Solid-state structure of (a) bare $K_2Fe_{22}O_{34}$, (b) Cr-doped $K_2Fe_{22}O_{34}$ with extra pillars in the interlayer space formed at low Cr doping, and (c) Fe_2O_3-domains in the interlayer space formed at high Cr doping.

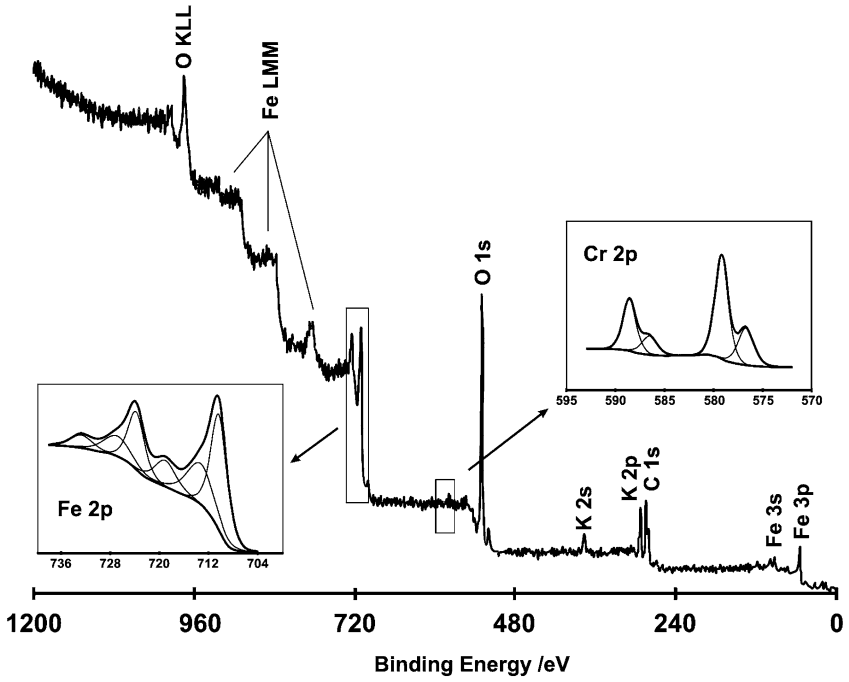

Fig. 5. XPS survey scan with the inserted narrow scans for Fe 2p and Cr 2p.

Table 2
XPS binding energies/eV for K 2p, Fe 2p, O 1s and Cr 2p in undoped and Cr-doped $K_2Fe_{22}O_{34}$

Sample	K $2p_{3/2}$	Fe $2p_{3/2}$	O 1s	Cr^{3+} $2p_{3/2}$	Cr^{6+} $2p_{3/2}$	Ref.
$K_2Fe_{22}O_{34}$	292.5	710.3	529.6	–	–	This work
	293.0	710.8	529.8	–	–	[a]
2% Cr-$K_2Fe_{22}O_{34}$	292.6	710.3	529.6	576.3	579.2	This work

[a] NIST Standard Reference Database 20; http://srdata.nist.gov/xps/elm_comp_res.asp.

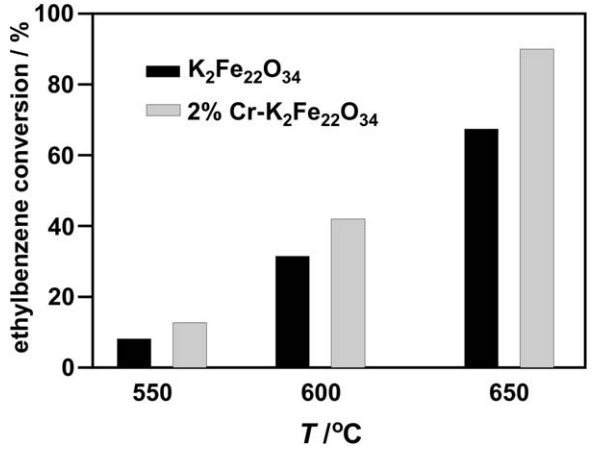

Fig. 6. Comparison of catalytic activity in ethylbenzene dehydrogenation for bare and 2% Cr-doped $K_2Fe_{22}O_{34}$.

temperatures investigated (550, 600, and 650 °C), the activity in terms of ethylbenzene conversion was distinctly higher for the Cr-doped sample, reaching 90% (in comparison with 67% for undoped ferrite) at the industrial process temperature. This catalytic activity is very similar to that observed for the real catalyst [28]. Besides the desired styrene monomer (observed with the yields of 76% for Cr-doped ferrite and 58.7% for undoped ferrite) and unreacted ethylbenzene, few byproducts (e.g., methane, ethylene, carbon dioxide, benzene, toluene) were detected. At 650 °C, their specific yields reached 0.7, 0.3, 4.8, 4.6, and 3.6% for the Cr-doped samples and 0.4, 0.4, 2.2, 3.6, and 2% for the undoped samples. Consequently, it may be concluded that the beneficial role of chromium additive observed previously for the real catalysts may be associated with the β-ferrite component. Having verified the positive role of chromium promoter on the catalyst performance, we next evaluated its effect on potassium stability in more detail.

3.3. Potassium thermal desorption

A comparison of K and K^+ desorption fluxes from undoped and 2% Cr-doped β-ferrites is shown in Fig. 7. For both samples, the atomic flux overwhelmed the ionic flux, which means that the main channel of potassium loss from the catalyst is due to atoms. Thus, the loss of potassium can be considered a volatilization process. According to the Saha–Langmuir equation [29], the probability of the ratio of ionic and neutral fluxes (j_+/j_0) from the surface is given by

$$\frac{j_+}{j_0} = \frac{g_0}{g_+}\exp\left[-\frac{e(V-\Phi)}{k_B T}\right],$$

where g_+/g_0 is the ratio of the statistical weights of the ionic and atomic states for potassium equal to 1/2; and e, V, Φ, k_B,

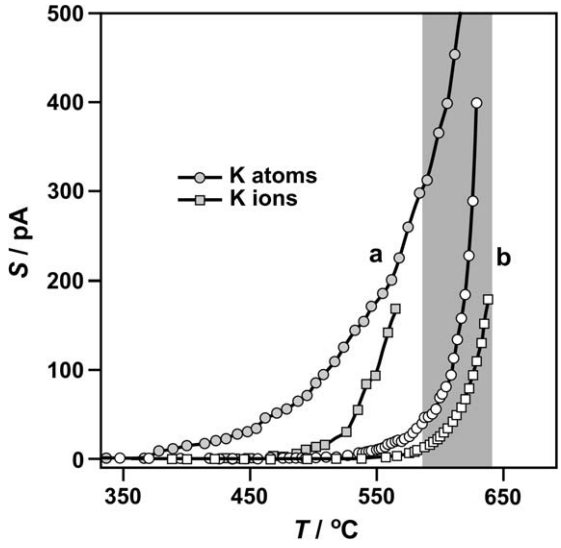

Fig. 7. Suppression of atomic and ionic desorption fluxes from $K_2Fe_{22}O_{34}$ phase upon 2 wt.% addition of Cr. The ionic signal from undoped sample is multiply by 100. The grey rectangle represents the temperature range of industrial styrene synthesis.

and T denote elementary charge, ionization potential of desorbing atom, work function of the surface, Boltzmann constant, and temperature, respectively. The domination of the atomic flux in the desorption process indicates that the work function of the samples must be <4.3 eV (the ionization potential of potassium). Indeed, the work function for the $K_2Fe_{22}O_{34}$ ferrite determined in parallel experiment of electron thermionic emission was 2.2 eV.

For the undoped β-ferrite, onset of the appreciable K desorption was observed at temperatures below 400 °C, whereas for Cr-substituted ferrite it was shifted to about 550 °C. The monotonous exponential changes of the signal with temperature indicate that in each case the potassium leaves the surface effectively trough a single potential barrier. Thus, the corresponding desorption energies were determined from the linear part of the Arrhenius-like plots ($\ln S$ vs $1/T$) for potassium atoms and ions (Fig. 8). The values are given in Table 3.

The desorption energy for potassium atoms changes from 0.83 ($K_2Fe_{22}O_{34}$) to 2.23 eV on doping with 2% Cr. This difference in desorption energetics is reflected in the dramatic quenching of the potassium volatilization gauged by the K flux intensity (Fig. 7). For ionic flux, the desorption energies are significantly higher, ranging from 2.33 for $K_2Fe_{22}O_{34}$ to 3.47 eV for 2% Cr-$K_2Fe_{22}O_{34}$. The lower desorption energies for atoms and the resulting domination of the atomic fluxes are characteristic of oxide surfaces in the temperature range studied [30]. The activation energies obtained can account for the desorption of potassium from the catalyst surface along several energetic pathways, leading to ionic and atomic potassium in different final states (e.g., 4s, 4p, 3d) outside the surface [20].

Chromium plays a beneficial role not only in the enhanced styrene yield of the β-ferrite, but also in the stabilization of potassium in this key phase. It is then important that in the course of catalyst formation, the Cr dopant is incorporated only into the β-ferrite component phase of the active catalyst. In-

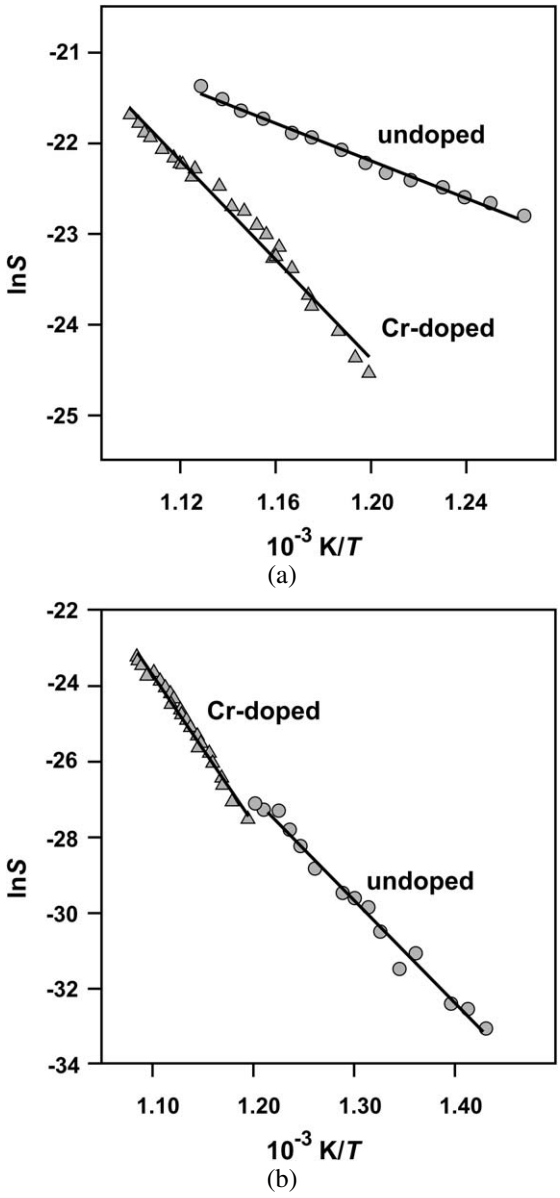

Fig. 8. Arrhenius plots for potassium desorption from undoped and 2% Cr-doped $K_2Fe_{22}O_{34}$ ferrite (a) atoms and (b) ions.

deed, parallel studies of potassium desorption from $KFeO_2$ – the second important phase of the styrene catalyst – revealed that Cr doping had the opposite effect on K stability; the desorption barrier for potassium atoms decreased dramatically, from 2.84 ± 0.06 eV for bare $KFeO_2$ to 1.16 ± 0.04 eV for 2% Cr-$KFeO_2$ [31].

The thermal desorption method used in this study allows for quick characterization of potassium stability and thus can be used as a time-saving alternative to the screening test of potassium volatilization from the styrene catalysts.

3.4. Solid-state model of Cr-doped β-ferrite

The crystal structure of potassium β-ferrite has been determined previously [32,33]. As already mentioned, it consists of Fe^{3+} ions in tetrahedral and octahedral coordination that form

Table 3
Activation energies, E_d (eV), for K and K^+ desorption from bare and Cr-doped $K_2Fe_{22}O_{34}$ potassium ferrites[a]

Sample	E_d (K)	E_d (K^+)
$K_2Fe_{22}O_{34}$	0.83 ± 0.01[b]	2.33 ± 0.03[b]
0.1% Cr-$K_2Fe_{22}O_{34}$	3.61 ± 0.03	3.07 ± 0.03
0.25% Cr-$K_2Fe_{22}O_{34}$	3.47 ± 0.02	3.38 ± 0.01
1% Cr-$K_2Fe_{22}O_{34}$	2.04 ± 0.015	1.80 ± 0.01
2% Cr-$K_2Fe_{22}O_{34}$	2.87 ± 0.01	3.60 ± 0.01
5% Cr-$K_2Fe_{22}O_{34}$	2.00 ± 0.01	–

[a] The energies were calculated for the correlation coefficient higher that 0.98 and the errors correspond to 95% confidence limit.
[b] From Ref. [16].

spinel blocks, but with 75% of the oxygen ions missing in every fifth layer. The remaining oxygen ions form *Fe3–O5–Fe3* pillars separating the spinel blocks in the c direction (Fig. 4a). The interlayer space is filled with loosely bound K^+ ions distributed in three distinct sites located on the (001) plane: Beevers–Ross (BR), anti-Beevers–Ross (aBR), and mid-oxygen (mO), as shown in Fig. 9 [17]. The K^+ ions (black circles) are able to move very easily, because there are more sites available than there are K^+ ions to occupy them. Thus, potassium ions are able to move rather freely within the conduction planes, but cannot penetrate within the dense spinel blocks. The dotted line in Fig. 9 indicates one possible pathway of interlayer diffusion to the external surface, through a series of hops between adjacent BR, mO, and aBR sites [34].

Evaluation of the Mössbauer data collected in Table 1 reveals that the ratio of octahedral to tetrahedral sites occupied by iron systematically decreased with Cr doping from 1.86 for the parent ferrite to 1.70 for the 2% Cr-doped sample and 1.38 for the 5% Cr-doped sample. Taking into account the significant difference in the stabilization energies of Cr^{3+} in O_h (CFSE = 224.5 kJ mol^{-1}) and in T_d (CFSE = 66.9 kJ mol^{-1}) crystal fields of oxides [35], it can be reasonably assumed that Cr^{3+} ions are located in the octahedral sites. This is in line with the well-known facts that all chromates contain octahedral Cr^{3+} and form normal spinels. Even such ions as Ni^{2+}, with large excess octahedral stabilization energy (86.2 kJ mol^{-1}), are forced into T_d sites in $NiCr_2O_4$ [36]. Analysis of the Mössbauer spectra reveals that occupation of the *Fe1* position by iron decreases and occupation of the *Fe3* position increases on chromium doping. Therefore, it can be inferred that Cr^{3+} ions substitute for Fe^{3+} (*Fe1*), which are displaced to *Fe3* sites located in the interlayer space (Fig. 4b). This is tantamount to the formation of new pillars in the interlayer space, where the loose potassium ions are located. Because the potassium transport channels are narrow (in fact, comparable to the size of potassium ions), such extra pillars provide steric obstacles that effectively block K diffusion (Fig. 9).

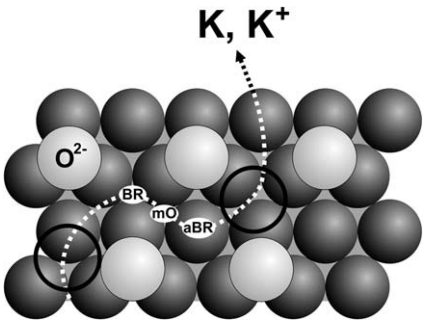

Fig. 9. Example of a interlayer diffusion pathway of potassium in (001) conduction plane of $K_2Fe_{22}O_{34}$. Once the external surface is reached desorption of potassium takes place.

With increased Cr doping, α-Fe_2O_3 domains (Fig. 4c) are formed, as indicated by XRD and Mössbauer spectra. When the concentration of pillars reaches a critical value, transformation of Fe^{3+} from the tetrahedral sites *Fe3* of extra pillars into octahedral sites of α-Fe_2O_3 domains most likely occurs through the formation of a maghemite (γ-Fe_2O_3) intermediate. Indeed, maghemite can be considered an Fe^{2+}-deficient spinel with the formula $(Fe^{3+}{}_8)_T[Fe^{3+}{}_{40/3}\square_{8/3}]_O O_{32}$, where $\square$ represents a vacancy, T indicates tetrahedral sites, and O represents octahedral sites. Thus, a meghemite structure can be formed at the interface region by association of the *Fe3* tetrahedra (pillars) with the *Fe1* octahedra of the β-ferrite blocks. Subsequent conversion of maghemite into hematite in the course of calcination occurs quite easily [37].

Although the resultant nuclei of α-Fe_2O_3 domains are initially formed in the interlayer space on Cr doping (Fig. 4) in the high-temperature regime of the synthesis (1470 K for 5 h), they can readily grow in three dimensions and eventually segregate as a separate hematite phase. This effect is particularly pronounced for higher Cr doping (2–5%), and in fact the α-Fe_2O_3 phase was observed in XRD and Mössbauer spectra for such samples (Figs. 1 and 3).

The extra-pillars potassium-blocking model provides a straightforward explanation for potassium stabilization by doping with other divalent and trivalent ions, such as Mg^{2+}, Mn^{2+}, and Al^{3+}. These ions may either displace the octahedral iron into tetrahedral sites to form the blocking pillars or occupy the tetrahedral sites in the interlayer space to create the pillars directly. The particular mechanism depends to a great extent on the crystal field stabilization preference and ionic radius constraints.

In the wet conditions of the real process, potassium is eventually removed from the catalyst in the form of KOH. This concept, originally advanced by Mross [38] and supported by Schlögl et al. [39], can be easily reconciled with our results. Our solid-state model accounts for diffusion of constitutional potassium from the bulk of the ferrite and subsequent desorption from the external surface. In the presence of water, potassium is then readily transformed into KOH, and, due to the rather high vapor pressure (∼0.1 mbar), is transported in this form along the reactor at the reaction temperature. This is in line with the fact that the spent catalyst surface consists mainly of iron oxide decorated with KOH [3,16]. Inhibition of potassium diffusion toward the surface by Cr doping prevents the undesired KOH formation. An optimal surface concentration of potassium can be achieved by appropriately adjusting Cr doping.

4. Conclusion

The stabilization of $K_2Fe_{22}O_{34}$ (the key phase of the active styrene catalyst) by chromium was investigated by the thermal desorption of potassium atoms and ions. The addition of chromium significantly increased K and K^+ desorption energies (by 1.4 and 1.1 eV, respectively) and reduced the flux of potassium volatilization by an order of magnitude. Our extra-pillars potassium-blocking model with Cr^{3+} displacing Fe^{3+} from octahedral to tetrahedral sites located in the interlayer space accounts for the observed potassium stabilization effect.

Acknowledgments

This work was sponsored by the Polish Committee for Scientific Research under Research Project 3 T09B 140 26. The authors thank Maria Sojka for preparing the artwork.

References

[1] M. Pugh, The Outlook of Polystyrene on The Third European Aromatics and Derivatives Conference, Antwerp, 2004.
[2] D. Resasco, in: I.T. Horvath (Ed.), Encyclopedia of Catalysis, vol. 3, Wiley, Hoboken, 2003, p. 76.
[3] G.R. Meima, P.G. Menon, Appl. Catal. A: Gen. 212 (2001) 239.
[4] K.K. Kearby, US Patent 2,426,829 (1947).
[5] B.D. Herzog, H.F. Raso, Ind. Eng. Chem. Prod. Res. Dev. 23 (1984) 187.
[6] T. Hirano, Appl. Catal. 26 (1986) 81.
[7] S.E.H. Elsanashaie, B.K. Abdallah, S.S. Elshishini, S. Olkowalter, M.B. Noureldeen, T. Aboudani, Catal. Today 64 (2001) 151.
[8] K. Kochloefl, in: G. Ertl, H. Knözinger, J. Weitkamp (Eds.), Handbook of Heterogeneous Catalysis, vol. 5, VCH, Weinheim, 1997, p. 2151.
[9] A. Trovarelli, C. De Leitenburg, M. Loaro, G. Dolcetti, Catal. Today 50 (1999) 353.
[10] T. Hirano, Appl. Catal. 28 (1986) 119.
[11] M. Muhler, J. Schütze, M. Wesemann, T. Rayment, A. Dent, R. Schlögl, G. Ertl, J. Catal. 126 (1990) 339.
[12] A. Miyakoshi, A. Ueno, M. Ichikawa, Appl. Catal A: Gen. 216 (2001) 137, and 219 (2001) 249.
[13] A. Kotarba, I. Kruk, Z. Sojka, J. Catal. 221 (2004) 650.
[14] M. Muhler, R. Schlögl, G. Ertl, J. Catal. 138 (1992) 413.
[15] G. Ketteler, G. Ranke, R. Schlögl, J. Catal. 212 (2002) 104.
[16] A. Kotarba, I. Kruk, Z. Sojka, J. Catal. 211 (2002) 265.
[17] S. Ito, H. Kurosawa, K. Akashi, Y. Michiue, M. Watanabe, Solid State Ionics 86 (1996) 745.
[18] L. Holmlid, K. Engvall, C. Aman, P.G. Menon, Stud. Surf. Sci. Catal. 75 (1992) 795.
[19] K. Engvall, L. Holmlid, Appl. Surf. Sci. 55 (1992) 303.
[20] L. Holmlid, P.G. Menon, Appl. Catal. 212 (2001) 247.
[21] A. Kotarba, A. Barański, S. Hodorowicz, J. Sokołowski, A. Szytuła, L. Holmlid, Catal. Lett. 67 (2000) 129.
[22] K. Engvall, L. Holmlid, A. Kotarba, J.B.C. Pettersson, P.G. Menon, P. Skaugset, Appl. Catal. A: Gen. 134 (1996) 239.
[23] K. Edstrom, S. Ito, R.G. Delaplane, J. Magn. Mater. 212 (2000) 347.
[24] K. Jiang, J. Yang, B. Hu, X. Yang, L. Mao, Y. Yuan, G. Zhang, Hyper. Inter. 111 (1998) 45.
[25] C.R. Brundle, T.J. Chuang, K. Wandelt, Surf. Sci. 68 (1977) 459.
[26] Z. Sojka, K. Klier, J. Electron. Spectrosc. Relat. Phenom. 60 (1992) 155.
[27] K. Wandelt, Surf. Sci. 1 (1982) 2.
[28] S.S.E.H. Elnashaie, B.K. Abdullah, S.S. Elshishini, S. Alkhowaiter, M.B. Noureldeen, T. Alsoudani, Catal. Today 64 (2001) 151.
[29] G.A. Somorjai, Introduction to Surface Chemistry and Catalysis, John Wiley & Sons, New York, 1994, p. 376.
[30] T.E. Madey, B.V. Yakshinsky, V.N. Ageev, R.E. Johnson, J. Geophys. Res. 103 (1998) 5873.
[31] I. Serafin, A. Kotarba, Z. Sojka, manuscript in preparation.
[32] J.P. Boilot, P.H. Colomban, G. Colin, R. Comes, Solid State Ionics 1 (1980) 69.
[33] S. Ito, S. Nariki, K. Kozawa, T. Uchida, Solid State Ionics 72 (1994) 300.
[34] A.K. Cheetham, P. Day, Solid State Chemistry Techniques, Clarendon Press, Oxford, 1987.
[35] J.D. Dunitz, L.E. Orgel, Adv. Inorg. Radiochem. 2 (1960) 1.
[36] A.R. West, Basic Solid State Chemistry, Wiley, Chichester, 1996.
[37] U. Schwertmann, R.M. Cornell, Iron Oxides in the Laboratory, VCH, Weinheim, 1991.
[38] W.D. Mross, Catal. Rev. Sci. Eng. 24 (1983) 591.
[39] O. Shekhah, W. Ranke, R. Schölgl, J. Catal. 255 (2004) 56.